

# Solar-cycle precursors and predictions

Jie Jiang

Key Laboratory of Solar Activity, National Astronomical Observatories,  
Chinese Academy of Sciences, Beijing 100012, China  
email: jiejiang@nao.cas.cn

**Abstract.** The sunspot number data during the past 400 years indicates that both the profile and the amplitude of the solar cycle have large variations. Some precursors of the solar cycle were identified aiming to predict the solar cycle. The polar field and the geomagnetic index are two precursors which are received the most attention. The geomagnetic variations during the solar minima are potentially caused by the solar polar field by the connection of the solar open flux. The robust prediction skill of the polar field indicates that the memory of the dynamo process is less than 11 yrs based on the frame of the Babcock-Leighton flux transport dynamo. One possible reason to get the short magnetic memory is the high magnetic diffusivity in the convective zone. Our recent studies show that the radial downward pumping is another possible reason. Based upon the mechanism, we well simulate the cycle irregularities during RGO time period. This opens the possibility to set up a standard dynamo based model to predict the solar cycle. In the end, the no correlation between the polar field and the preceding cycle strength due to two nonlinearities involved in the sunspot emergence will be stressed.

**Keywords.** Sun: magnetic fields, Sun: activity, (Sun:) solar-terrestrial relations

---

## 1. Introduction

Predicting the sunspot number began when a cyclical behavior was noticed by Schwabe. Long-term time series observations indicate that solar cycle amplitudes vary from cycle to cycle. This makes the solar cycle prediction appealing. Solar cycle predictions became important when we began putting assets in space that are directly affected by solar activity. Further motivation to predict solar cycle arises from the potential implications for understanding the origin of solar magnetic field. A reliable prediction method could provide a constraint on the dynamo mechanisms.

The paper is organized as follows. An introduction about the solar-cycle precursors with emphases on the geomagnetic variations and the polar field will be presented in Section 2. The dynamo mechanisms constrained by the polar field prediction skill will be given in Section 3. It is mainly about the flux transport mechanisms from the poloidal field generation layer to the toroidal field generation layer. Section 4 would be on the solar polar field generation which is related to the generation of the poloidal field from the toroidal field.

## 2. Solar-cycle precursors

A number of techniques are used to predict the amplitude of a cycle during the time near or before sunspot minimum. Precursor methods have been proved to be the most successful technique for solar activity predictions in the past. Precursor methods are based on the correlations between certain measured quantities in the declining phase of a cycle and the strength of the next cycle. The geomagnetic variation and the polar field are two precursors which are received the most attention due to their significant prediction skill.

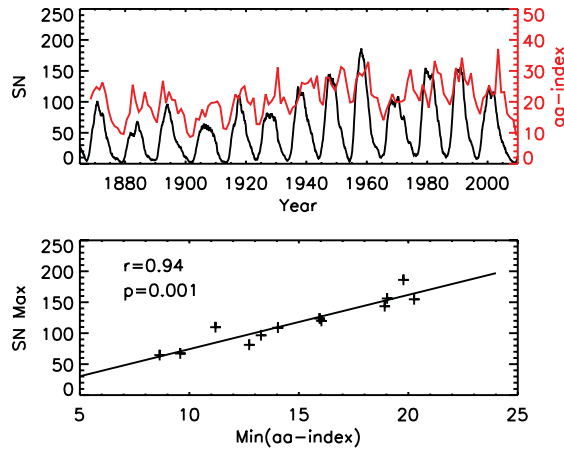


**Figure 1.** Geomagnetic variation precursor. Upper panel: time evolution of the 12-month smoothed group sunspot number (black curve) and the yearly aa-index (red curve). Lower panel: aa-index minimum of each cycle vs. maximum sunspot number of the subsequent cycle. The good correlation between them provides the based of the geomagnetic variation precursor.

### 2.1. Geomagnetic variation precursor

Geomagnetic variation precursor is based on the changes in the Earth's magnetic field. Geomagnetic indices are usually used to quantify the geomagnetic variations. The aa-index is the simplest three hourly global geomagnetic activity index (Mayaud, 1972). It is estimated on the data of two geomagnetic observatories, approximately antipodal. The main advantage in using aa-index is that its time series is the longest available among all the planetary indices, the first values dates back to 1868.

The upper panel of Figure 1 shows the time evolution of the yearly aa-index data † in red curve overplotted with 12-month smoothed group sunspot number in black curve since 1868 onwards. The lower panel shows the correlation between the minimum values of aa-index of each cycle with the subsequent sunspot number maximum. We may see the minimum of the aa-index is directly related to the maximum sunspot number for the following cycle. This provides the basis of geomagnetic variations precursor which was firstly proposed by Ohl(1966).

### 2.2. Physical reasons for the geomagnetic variations

Now let's see what causes the variation of aa-index. Left panel of Figure 2 shows the time evolution of the daily-averaged aa-index overplotted with the daily-averaged radial component of the interplanetary magnetic field (IMF) measured by OMNI ‡. We may see that they closely follow each other. Right panel shows their correlation, the coefficient of which reaches 0.8. Hence, aa-index variations are almost entirely due to variations in near-Earth radial IMF. This is consistent with the result given by Stamper *et al.*(1999) who analyzed the cause of the century-long increase in the aa-index using observations of interplanetary space, galactic cosmic rays, the ionosphere and the auroral electrojet.

The IMF is produced by the solar wind which drags some magnetic flux, corresponding to the solar open flux, out of the Sun to fill the heliosphere. The solid curve in Figure 3 is the solar open field derived by extrapolation of Mount Wilson (MWO) and Wilcox solar

† <http://www.leif.org/research/>  
 ‡ <http://omniweb.gsfc.nasa.gov/>

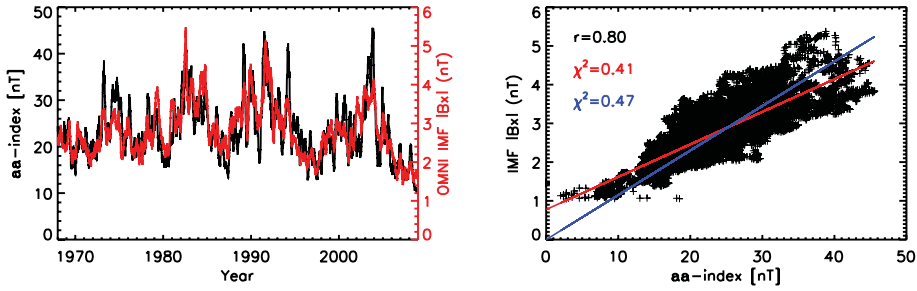


**Figure 2.** aa-index vs. radial component of the IMF. Left panel: time evolution of the daily averaged aa-index (black curve) overplotted with the daily averaged radial component of the IMF measured by OMNI (red curve) during 1968-2010. Right panel: correlation diagram of the aa-index and the radial IMF. The coefficient reaches 0.8.

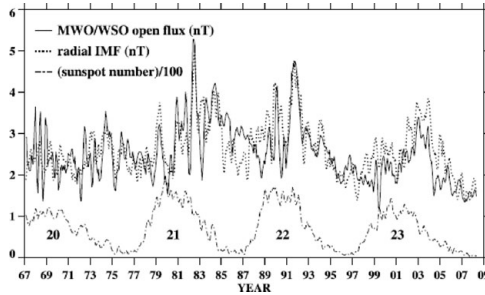


**Figure 3.** Comparison between the near-Earth radial IMF strength (dotted curve) and the total open flux, derived from a PFSS extrapolation of MWO and WSO magnetograph measurements and expressed as an equivalent field strength (nT) at 1 AU (solid curve). Also plotted is the sunspot number in solid and dotted curve (from Wang 2009).

(WSO) observatories magnetogram and the overplotted dashed curve is radial component of the IMF at 1AU (Wang & Sheeley 2009). They show reasonably good agreement both in its magnitudes and in the shape of its fluctuations. Hence the variation of the radial IMF is caused by the solar open field.

Now let us analysis the solar open field. The radial magnetic field outside of the solar surface is in the following form under the assumption of potential field,

$$B_r(r, \theta, \phi) = \sum_{l=0}^{\infty} \sum_{m=-l}^{m=l} c_l(r) a_{lm} Y_{lm}(\theta, \phi). \tag{2.1}$$

The coefficient  $c_l(r) \propto r^{-(l+2)}$  rapidly falls with  $l$ . Hence only the lowest-order multipoles contribute significantly to the field at the source surface and hence to the solar open flux. The lowest-order multipoles are the axial dipole field and the equatorial dipole field.

Red curve and blue curve in Figure 4 correspond to the time evolution of sunspot number and the open flux during 1900-2010, respectively. Black solid curve is the evolution of axial dipole field and black dashed curve is the evolution of equatorial dipole field. They are adapted from Jiang et al.(2011b) who physically reconstructed the solar total, polar and total flux since 1700 onward based on the semi-synthetic records of emerging sunspot groups (Jiang *et al.* 2011a). We may see that the axial dipole is roughly anti-phase with

the solar cycle which is similar to the polar field behavior and provides the most open flux near cycle minimum. The equatorial dipole field is roughly in phase with the solar cycle and provides the most open flux near cycle maximum.

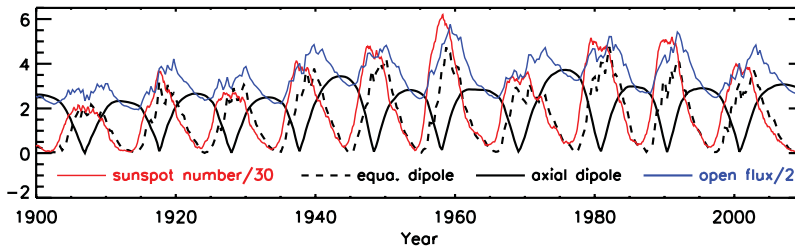


**Figure 4.** Reconstructed solar open flux (blue curve), equatorial dipole field (black dashed curve) and axial dipole field (black solid curve) since 1900 onward to show the relation between the equatorial and dipole field with the solar cycle. Also plotted is the sunspot number in red curve (adapted from Jiang *et al.*, 2011b using the semi-synthetic records of emerging sunspot groups by Jiang *et al.*, 2011a).

Here is a summary about the physical reason for the geomagnetic (aa-index) variations. Solar magnetic field varies with the solar cycle. Solar wind drags some solar open magnetic field out of the Sun to form the IMF. The variation of the radial IMF causes the variation of geomagnetic (aa-) index which presents different behaviors during different phases of solar cycle. At the cycle maximum, aa-index reflects the strength of the solar cycle, which is dominated by the solar equatorial dipole field. At the cycle minimum, aa-index reflects the strength of the polar field, which is dominated by the solar axial dipole field. Hence the behavior of the aa-index around the solar minima is consistent with the polar field around the solar minimum. In fact, the minimum values of aa-index always 1-2 yr lag behind the epoch of the solar minimum (Du *et al.*, 2009). This is mainly due to the decay of the equatorial dipole field on a timescale of 1yr, see Wang & Sheeley (2002, 2009) for details.

### 2.3. Solar polar field precursor

Solar polar field was first proposed to be solar cycle precursor by Schatten *et al.*(1978), who suggested the correlation between the polar field near the solar minimum and the subsequent cycle strength. WSO has the continuous solar polar field observations since 1976 shown in Figure 5 (red curve) overplotted with the sunspot number †. The left panel of Figure 6 gives the relation between the directly observed maximum polar field of cycle  $n$  and the subsequent cycle  $n + 1$  strength. Cycle 24 is included in using the predicted strength by Jiang *et al.*(2007). These 4 points distribute closely along the straight line which hints the good correlation between the polar field and the cycle strength.

However the 4 cycle data are less convincing to demonstrate the correlation. We need longer time series data. Surface flux transport (SFT) model is an effective way to reconstruct solar polar magnetic field with the input of sunspot group data (Wang *et al.* 1989; Schrijver *et al.* 2002; Mackay *et al.* 2002; Baumann *et al.* 2004). CJSS10 used the SFT model to reconstruct the surface field and open flux for the period 1913-1986. The observed sunspot longitudes, latitudes, areas and cycle-averaged tilt angles were used to create the source term. The results of that model compare well with the open flux

† <http://wso.stanford.edu/Polar.html>

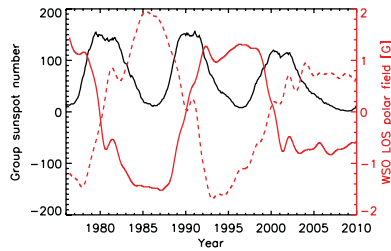


**Figure 5.** Time evolution of the line-of-sight solar polar field observed by WSO since 1976 (south pole: red dashed curve, north pole: red solid curve). Sunspot number is overlotted in black curve.

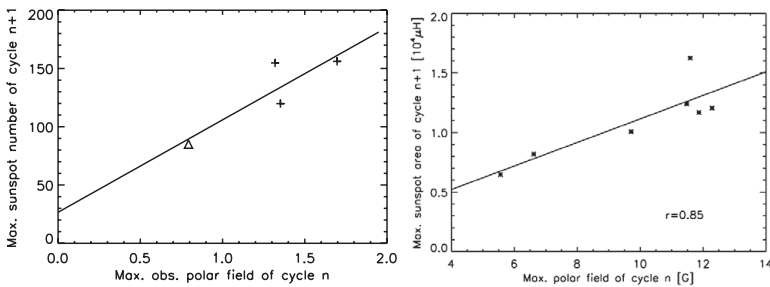


**Figure 6.** Correlations between the maximum polar field near the end of solar cycle  $n$  and the maximum strength of cycle  $n+1$ . Left: observed polar field during cycles 21–23 (LOS component, averaged over  $35^\circ$  wide polar caps). Right: reconstructed polar field during cycles 15–21 (radial component, averaged over the  $15^\circ$  wide polar caps, from Cameron *et al.*, 2010).

derived from geomagnetic indices (Lockwood 2003) and the reversal times of polar fields (Makarov *et al.* 2003). Right panel of Figure 6 shows the correlation between the reconstructed polar field maximum during the end of the cycles 15–21 and the subsequent cycle strength. They show the strong correlation with the correlation coefficient 0.85. Please note that different definitions of the polar field were used between the observation (left panel, line-of-sight component and averaged over  $35^\circ$  wide polar caps) and the reconstruction (right panel, radial component and averaged over the  $15^\circ$  wide polar caps). Jiang *et al.* (2011c) show that they are consistent when the same definitions are used. The good correlation provides the evidence for the polar field to be the solar cycle precursor.

The polar field is the polar component of the solar poloidal field which is one part of the dynamo loop since the dynamo model is regarded as the oscillation between the poloidal field and the toroidal field (Parker, 1955). The toroidal field usually is corresponding to the cycle strength. The polar field and the cycle strength are connected by the solar dynamo process. Their correlation given by the direct or the indirect observations hence would provide constraints on the solar dynamo.

Except the former mentioned explanation of the aa-index prediction skill which provides the constraint on the solar dynamo. There is an alternative explanation given by Cameron & Schüssler (2007). We know that stronger cycles rise faster toward sunspot maximum. It is the Waldmeier effect. Moreover, the high-latitude spots of the new cycle already appear when the old cycle is still in progress in low latitudes. It is the cycle overlapping. The two properties of the sunspot record were used to explain the precursor skill. A stronger follower cycle with a shorter rise time leads to an earlier minimum and

a higher predictor than a weaker subsequent cycle with a longer rise time. Thus the minimum epoch and height depend on the strength of the following cycle. Hence no physical connection between the surface manifestations of subsequent activity cycles is required in this explanation.

### 3. Dynamo mechanisms constrained by the polar field precursor

#### 3.1. Possible reasons responsible for the polar field precursor

Section 2 has shown that the aa-index precursor is consistent with the polar field precursor since the aa-index at the solar minimum roughly reflects the strength of polar field maximum by the connection of the axial dipole component of the open flux. Their prediction skill provides the constraint on the solar dynamo models. Let's see the constraints that the precursor skill can give. The following discussion is based on the Babcock-Leighton (BL)-type flux transport (FT) dynamo. See Choudhuri (2013) in this proceeding for more details about the BL-type FT dynamo.

Although the correlation between the polar field maximum and the subsequent cycle strength was proposed by Schatten *et al.* (1978) based on the BL-type FT dynamo, here we would like to stress that not all BL-type FT dynamo can give the correlation. In the BL-type dynamo, poloidal field is generated at surface layer due to the decay of the tilt sunspot groups. Toroidal field corresponding to the subsequent cycle strength locates in the tachocline at the base of the convection zone. It means that the toroidal and the poloidal field are spatial separated. There are two possibilities illustrated by Figure 7 to generate the correlation between two spatial separated parameters.

During a maximum, the poloidal field created by the BL process is primarily in mid-latitudes of the surface layer denoted as **C** in Figure 7. Left panel shows one possibility. The poloidal field is transported to the polar region **P** to produce the polar field which reaches the maximum near the solar minimum. Later it is then advected downward to the tachocline, where it is stretched by the differential rotation to create the toroidal field. The correlation between the polar field at the minimum and the strength of the next maximum can be explained if this polar field can be brought to the mid-latitude tachocline (denoted by **T**) in order of 5 yrs, which serves as the constraint of the dynamo model. The right panel show the other possibility. When the poloidal field at **C** produced during a maximum is swept away from **C** polewards to **P** to form the polar field, it is

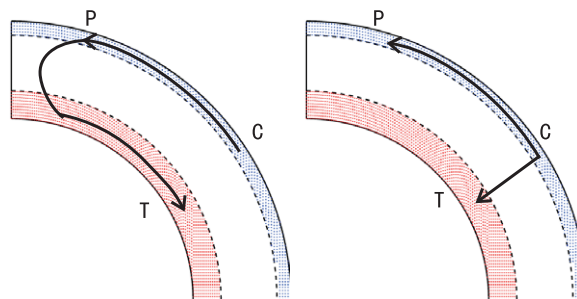


**Figure 7.** Cartoon to illustrate the possibilities causing the correlation between the polar field (denoted as **P**) and the next cycle strength (denoted as **T**). The blue and red region show the location of the poloidal and the toroidal field generation, respectively. Left panel: the poloidal field generated at the middle latitudes of the surface (denoted as **C**) is first transported to the pole and later to the tachocline. Right panel: the poloidal field at **C** is poleward transported to the pole and inward transported to the tachocline simultaneously.

simultaneously inward transported to the tachocline at **T**. The same cause, poloidal field at **C** causes the correlation between polar field maximum and the strength of the next maximum. The constraint in this possibility is that about 5 yrs is required for the flux at **C** to transport to **P** and **T**, respectively.

### 3.2. Three classes of BL-type FT dynamo models and the comparisons with the precursor constraint

Meridional flow, turbulent diffusivity and convective pumping are three potential mechanisms which are responsible for the transport of the poloidal field from the solar surface to the tachocline. The convective pumping was once ignored by the past dynamo studies. Yeates *et al.* (2008) distinguished the previous BL-type FT dynamo as the advection (meridional flow) and the diffusion dominated models. Cameron *et al.* (2012) indicated the downward pumping of magnetic flux has a significant effect in slowing the diffusive transport of magnetic flux through the solar surface. Provided the pumping was strong enough, the FT dynamo using a vertical boundary condition matches the SFT model. This study is supposed to be the prelude to initiate the pumping dominated BL-type FT dynamo models.

In the following we list some typical models of each class and analyze that whether each class is consistent with the precursor constraints. The meridional flow is a basic ingredient in all the BL-type FT dynamo models. Helioseismology has few knowledge on the equatorwards meridional flow in the solar interior. Hence different profiles were adopted in the dynamo models. In spite of the differences, there is no much difference for the poloidal field to be transported to the bottom under the sole advection of the meridional flow. It is about 2 cycles for all the models.

#### 3.2.1. Meridional flow dominated class

The dynamo models aiming for the solar cycle prediction used in Dikpati *et al.* (2006a, 2006b) belong to the meridional flow dominated class. Turbulent diffusivity in their model is in the range of  $3 \times 10^{10} - 2 \times 10^{11} \text{cm}^2 \text{s}^{-1}$ . It takes more than 5 solar cycles for the poloidal field at the surface to diffuse all the way to the bottom. No convective pumping was considered. Hence the transport mechanisms in their models are the meridional flow dominated.

Due to the advection of the meridional flow, the poloidal field is transported to the poles to form the polar field and later to the tachocline where it is stretched to form the toroidal field. This is consistent with the first possibility mentioned in the last section (left panel of Figure 7). However, it takes 17-21 years for the meridional flow to take the polar field to the tachocline. Hence it causes the correlation between polar field and the strength of the cycle after the next. Obviously, this is not consistent with the polar field precursor constraint.

#### 3.2.2. Turbulent diffusivity dominated class

Another group of dynamo based solar cycle prediction models are turbulent diffusivity dominated. They are Choudhuri *et al.* (2007) and Jiang *et al.* (2007), see also Chatterjee *et al.* (2004). The turbulent diffusivity is in order of  $10^{12} \text{cm}^2 \text{s}^{-1}$ . Just about 5 yrs are required for the poloidal field at the surface to diffuse to the bottom. Hence the models belong to the turbulent diffusivity dominated class.

When the poloidal field is advected to the pole under the effect of the meridional flow and the turbulent diffusivity to form the polar field, the poloidal field is diffused to the tachocline simultaneously mainly due to the high diffusivity. This is consistent with the second possibility in the last section (right panel of Figure 7). The transport

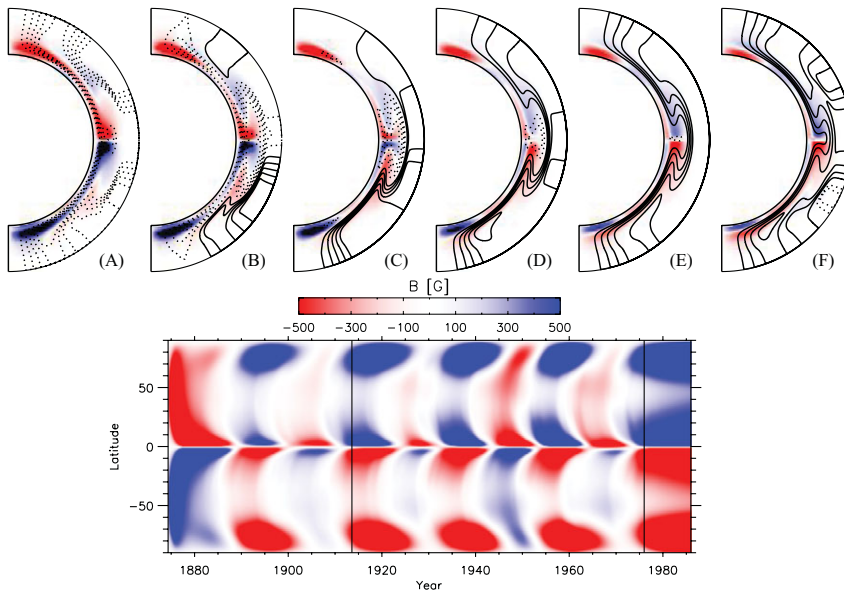


**Figure 8.** Results from the turbulent pumping dominated model in Jiang *et al.* (2012). Top panel: variation of the magnetic field over solar cycle 19. The red and blue colors correspond to negative and positive toroidal flux respectively, the lines are field lines based on the poloidal flux. The times (A)-(F) correspond to  $t = 1957.9, 1959.8, 1961.7, 1963.6, 1965.5$  and  $1967.4$  respectively. Lower panel: toroidal field at the base of the convection zone (integral over  $0.65 < r/R_{\odot} < 0.75$ ). The two vertical lines indicate the period for which cycle-averaged tilt angle observations during the RGO record are available.

time from the surface middle latitudes to the pole and to the tachocline are both about 5 yrs. Thus in the model, the polar field at the solar minimum has a strong correlation with the subsequent cycle strength. Obviously, the result shown in this group of models is consistent with the polar field precursor which provides a possibility for the surface poloidal flux transport to the tachocline.

### 3.2.3. Turbulent pumping dominated class

Recently people become aware of the effects of turbulent pumping in the BL-type FT dynamo. Guerrero & de Gouveia Dal Pino (2008), Cameron *et al.* (2012), Karak & Nandy (2012) and Jiang *et al.* (2012) have shown the importance of the turbulent pumping in their models. In the following I take Jiang *et al.* (2012) as an example to show how pumping works in the FT dynamo models.

In Jiang *et al.* (2012), the magnetic pumping extends to the base of the convection zone with the strength  $2\text{ms}^{-1}$  in the convection zone. Near the surface, it reaches  $20\text{ms}^{-1}$  which is consistent with the constraint of Cameron *et al.* (2012) to prevent the diffusive transport of magnetic flux through the solar surface. Less than 5 yr is required for the poloidal field at the surface to be transported to the bottom under the sole effect of turbulent pumping. Hence the transport mechanism in the model is pumping dominated. The turbulent diffusivity is  $2 \times 10^{11} \text{cm}^2 \text{s}^{-1}$ .

The poloidal source was based as closely as possible on the observations. The time evolution of the magnetic field through solar cycle 19 is shown in the upper panel of Figure 8. The transport of poloidal flux from the surface to the tachocline occurs over the same time span as the flux is transported to the poles. Throughout the cycle both the poloidal and toroidal fluxes have a simple form, i.e. no remnants from previous cycles.

In lower panel of Figure 8 we see equatorward propagating toroidal flux at low latitudes. The maxima of the modeled activity levels derived by the integration of the toroidal flux at the base of the convective zone between  $r = 0.65R_{\odot}$  and  $r = 0.75R_{\odot}$  and over latitudes  $-45^{\circ} < \lambda < 45^{\circ}$  are clearly related to the amplitude of the observed cycles. The correlation coefficient is above 0.8. The surface evolution of the field is similar to that given by the surface flux transport model. The correlation between the polar fields and the strength of the next cycle is above 0.8 as well.

Hence the results from the model with the pumping dominated transport mechanism is consistent with the polar field precursor as well. Being the same as the high turbulent diffusivity, the turbulent pumping provides the other possibility to dominate the transport of the surface poloidal flux to the bottom.

## 4. Solar polar (surface poloidal) field generation

### 4.1. Overview of the polar field generation

Sections 2 and 3 have shown the importance of the solar surface poloidal field which could bridge the observations with the BL-type FT dynamo models. As the polar component of the poloidal field, solar polar field is a direct observational quality (the consistent measurement started from 1976 as mentioned before). Now we analysis the polar field generation which is related to the solar poloidal field generation.

Left panel of Figure 9 is the maximum values of the observed polar field (from WSO) at the end of each solar cycle verse the maximum sunspot number of the same cycle during cycles 20-23. Right panel is the reconstructed solar polar field from Cameron et al. (2010) verse the maximum sunspot areas of the same cycle during cycles 15-20. Being contrary to Figure 6, we may see that there is no correlation between the polar field and the same cycle strength.

The evolution of the solar polar field may be described as follows. The eruption of bipolar sunspot groups with their leading polarities systematically equatorward of their following polarities establishes an overall separation of polarities in latitudes. Differential rotation and surface diffusion separate the two polarities further. The flux of leading polarities decays around the equator due to the effect of diffusion. Meridional flow and the turbulent diffusion transport the net flux of the following polarities in each hemisphere to the poles to reverse the polar field of old cycle and build up the polar field of new cycle. In a word, the tilt sunspot group emergence provides the source of the solar polar field which is determined by the number and the properties of the sunspot group emergence. The nonlinearities and the randomness are involved in the sunspot group emergence, which will be presented in the following. Eventually, the polar field strength is dominated by the cross-equator net flux during the evolution of the solar cycle.

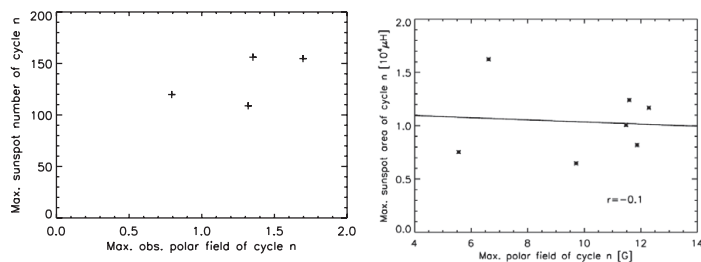


**Figure 9.** Same as Figure 6, but for the correlations between the polar field and the same cycle strength, which shows no correlation.

#### 4.2. Nonlinearities in the polar field generation

Jiang *et al.* (2011a) studied the statistical properties of sunspot group emergence on the cycle phase and strength. One of their results shown in Figure 10 gives the correlation between cycle averaged latitudes of sunspot emergence and cycle strength defined by the maximum sunspot number. We see that strong cycles tend to have higher mean latitudes for sunspot group emergence. High mean latitude for sunspot group emergence generates less cross-equator flux, hence a weak polar field. This is one nonlinear mechanism to modulate the polar field generation for strong cycles.

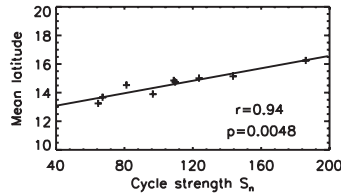


**Figure 10.** Correlation between cycle averaged latitudes of sunspot emergence and cycle strength defined by the maximum sunspot number during cycles 12-20 (from Jiang *et al.*, 2011a).

The tilt emergence (related to Joy's law) is a distinguished feature of sunspot groups. Left panel of Figure 11 shows the study from Dasi-Espuig *et al.* (2010) about the cycle averaged tilt angle normalized by the emergence latitude verse the strength of the same cycle. We see that the strong cycle corresponds to weak sunspot group tilts. Right panel of Figure 11 is the result from Baumann *et al.* (2004) about the polar field strengths and the sunspot group tilts which present a good linear relation. For weaker tilt angles, cross-equatorial cancelation of preceding flux is decreased leading to the accumulation of less flux at the poles. Hence the weaker tilt angles of sunspot groups for stronger cycles is another nonlinearity to modulate the solar polar field generation.

The two non-linear features of sunspot group emergence that the cycle averaged tilt angles are weaker and the mean latitudes are higher for the stronger cycles provide the explanation for the non-correlation between the polar field and the same cycle strength.

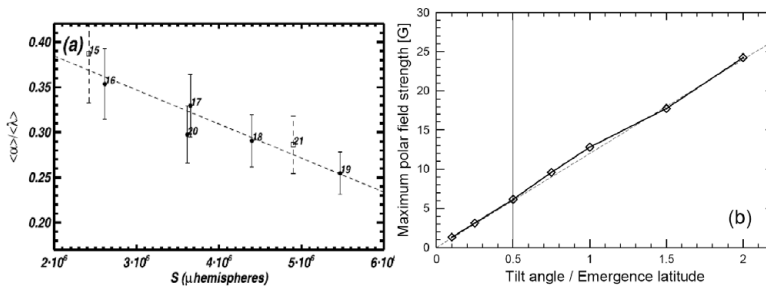


**Figure 11.** Nonlinearity in polar field generation caused by the tilt angles of sunspot group emergence. Left panel: cycle averaged tilt angle normalized by the emergence latitude vs. strength of the same cycle (from Dasi-Espuig *et al.*, 2010). Right panel: polar field strength vs. the tilt angles (from Baumann *et al.*, 2004).

#### 4.3. Randomness in the polar field generation

Except the nonlinearities, the polar field generation also involves in the random processes. The well anti-correlation between the tilt angle and the cycle strength shown in Figure 11 is a cycle averaged behavior. Left panel of Figure 12 shows the number density

distribution of the observed sunspot group tilts based on the MWO and Kodaikanal tilt angle data. We see the tilt angle value presents a large scatter probably due to the effect of convective flows on the flux tube emergence (Longcope & Fisher, 1996). Concerning the latitude distribution shown in right panel of Figure 12, the mean latitude at different phase of solar cycle denoted by the red curve may be given by a well defined second polynomial (see Jiang *et al.*, 2011). But the wide latitude distribution indicates the scattering distribution in the latitudes at given cycle phases. That how strongly these unpredictable random processes affect the polar field generation will be studied in our future work.

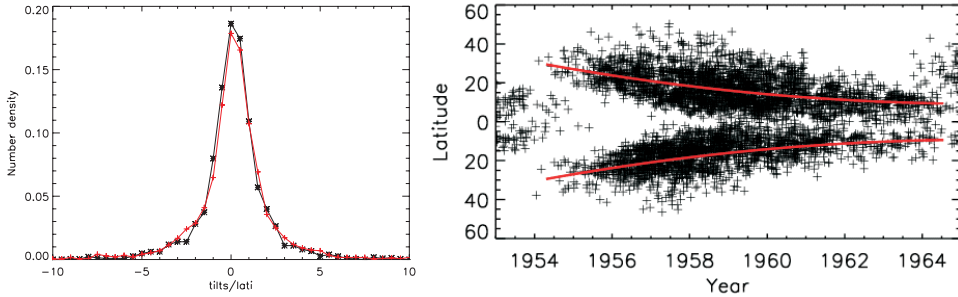


**Figure 12.** Randomness of the sunspot group emergence. Left panel: number density distribution of the sunspot group tilts based on the MWO (black) and Kodaikanal (red) tilt angle data; Right panel: latitude distribution during solar cycle 19. Red curve denotes the mean latitudes.

## 5. Conclusions

In the paper, I have a review of two major solar cycle precursors, the geomagnetic variations and the solar polar field. The physical reasons responsible for their precursor skill are presented. Further the constraints that the polar field precursor provide to the solar dynamo model are discussed and the physical mechanisms modulating the polar field generation are proposed. The main points can be concluded as follows.

1. The geomagnetic variation (the aa-index) precursor is consistent with the polar field precursor since the aa-index at the solar minimum roughly reflects the strength of polar field maximum by the connection of the axial dipole component of the open flux.

2. The polar field precursor hints that the transport of the poloidal field generated at the solar surface to the tachocline in less than one cycle, which provides a constraint on the flux transport mechanism. The BL-type FT dynamo models with the high turbulent diffusion (in order of  $10^{12} \text{cm}^2 \text{s}^{-1}$ ) or the turbulent pumping (in order of  $2 \text{ms}^{-1}$ ) satisfy the constraint.

3. Solar cycle strength is predictable at the end of old cycle since the generation of the toroidal field from the poloidal field is regarded as a deterministic process. However, the generation of the poloidal field is a complex process. Both nonlinear and random processes are involved in the sunspot emergence and further in the poloidal field generation, which may be the cause of the solar cycle irregularities. Other nonlinear and random processes are also possible involved which are unknown to us now.

## Acknowledgements

The author acknowledges the financial support from the National Natural Science Foundations of China (11173033, 11178005, 11125314) and the Knowledge Innovation Program of CAS (KJCX2-EW-T07).

## References

- Baumann, I., Schmitt, D., Schüssler, M., & Solanki, S. K. 2004, *A&A*, 426, 1075
- Cameron, R. & Schüssler, M. 2007, *ApJ*, 659, 801
- Cameron, R. H., Jiang, J., Schmitt, D., & Schüssler, M. 2010, *ApJ*, 719, 264
- Cameron, R. H. 2011, in: A. R. Choudhuri & D. Banerjee (eds.), *First Asia-Pacific Solar Physics Meeting* (ASI Conference Series), p. 143
- Cameron, R. H., Schmitt, D., Jiang, J., & İşik, E. 2012, *A&A*, 542, A127
- Chatterjee, P., Nandy, D., & Choudhuri, A. R. 2004, *A&A*, 427, 1019
- Choudhuri, A. R., Chatterjee, P., & Jiang, J. 2007, *Phys. Rev. Lett.*, 98, 131103
- Choudhuri, A. R., 2012, these proceedings
- Dasi-Espuig, M., Solanki, S. K., Krivova, N. A., Cameron, R. H., & Peñuela, T. 2010, *A&A*, 518, 7
- Dikpati, M., de Toma, G., & Gilman, P. A. 2006a, *Geophys. Res. Lett.*, 33, 5102
- Dikpati, M. & Gilman, P. A. 2006b, *ApJ*, 649, 498
- Du, Z. L., Li, R., & Wang, H. N. 2009, *AJ*, 138, 1998
- Guerrero, G. & de Gouveia Dal Pino, E. M. 2008, *A&A*, 485, 267
- Jiang, J., Chatterjee, P., & Choudhuri, A. R. 2007, *MNRAS*, 381, 1527
- Jiang, J., Cameron, R. H., Schmitt, D., & Schüssler, M. 2011a, *A&A*, 528, A82
- Jiang, J., Cameron, R. H., Schmitt, D., & Schüssler, M. 2011b, *A&A*, 528, A83
- Jiang, J., Cameron, R. H., Schmitt, D., & Schüssler, M. 2011c, *Space Sci. Revs*, 136
- Jiang, J., Cameron, R. H., Schmitt, D., & Isik, E. 2012, submitted
- Karak, B. B. & Nandy, D. 2012, ArXiv e-prints, 1206.2106
- Kitchatinov, L. L. & Olemskoy, S. V. 2011, *Ap. Lett.*, 37, 656
- Lockwood, M. 2003, *J. Geophys. Res.*, 108, 1128
- Longcope, D. W. & Fisher, G. H. 1996, *ApJ*, 458, 380
- Mackay, D. H., Priest, E. R., & Lockwood, M. 2002, *Solar Phys.*, 209, 287
- Makarov, V. I., Tlatov, A. G., & Sivaraman, K. R. 2003, *Solar Phys.*, 214, 41
- Mayaud, P.-N. 1972, *J. Geophys. Res.*, 77, 6870
- Ohl, A. I. 1966, *Soln. Dann.*, 12, 84
- Parker, E. N. 1955, *ApJ*, 122, 293
- Schatten, K. H., Scherrer, P. H., Svalgaard, L., & Wilcox, J. M. 1978, *Geophys. Res. Lett.*, 5, 411
- Schrijver, C. J., De Rosa, M. L., & Title, A. M. 2002, *ApJ*, 577, 1006
- Stamper, R., Lockwood, M., Wild, M. N., & Clark, T. D. G. 1999, *J. Geophys. Res.*, 104, 28325
- Wang, Y.-M. 2009, *Space Sci. Revs*, 144, 383
- Wang, Y.-M., Nash, A. G., & Sheeley, N. R., Jr. 1989, *ApJ*, 347, 529
- Wang, Y.-M. & Sheeley, N. R. 2002, *J. Geophys. Res.*, 107, 1302
- Wang, Y.-M. & Sheeley, N. R. 2009, *ApJ Lett.*, 694, L11
- Yeates, A. R., Nandy, D., & Mackay, D. H. 2008, *ApJ*, 673, 544